Hydroplaning during Steady-State Cornering Maneuvers

L. D. Metz
Metz Engineering and Racing, LLC

ABSTRACT

Vehicles running in wet conditions may experience hydroplaning of one or more tires. Hydroplaning can, and often does, change vehicle braking, acceleration and handling characteristics dramatically. Proper analysis of this behavior requires accommodating the clearing of paths for the rear tires that may result from the front tires engaging the water-coated surface first. In this work, tire overlap and associated hydroplaning behavior are theoretically & experimentally examined.

INTRODUCTION

In many accident situations involving inclement weather, hydroplaning is alleged to have initiated the loss of control and subsequent accident. Because a hydroplaning tire can experience a near-total loss of frictional capability, the driver of such a vehicle cannot exert control inputs at the hydroplaning tire/road interface large enough to recover from such a loss of control. From a vehicle dynamics and control point of view, the behavior of a hydroplaning tire is characterized by a drastic reduction in the radius of its friction circle.

Hydroplaning research has involved both theoretical [1-3] and experimental [4-10] studies. Experimental studies have involved testing of individual tires on drum and flat-track test machines, as well as towed tire and full-scale vehicle testing. Such testing is usually done on a skidpad, but occasionally is performed on an actual roadway surface. Individual tire testing on skidpads and roads has almost universally been conducted with the tire traveling in a straight line. The experimental studies involving individual tire testing on laboratory machinery and on roadway settings did much to improve understanding of the fundamental physics and behavior of a single tire under hydroplaning conditions, but provided little insight into the vehicle dynamics that might result from one or more hydroplaning tires. Studies involving full-scale vehicle testing, on the other hand, provided insight on the handling and braking effects of hydroplaning without little or no differentiation or insight into the behavior of individual tire(s).

It is well known that if a loss of traction due to hydroplaning occurs on the rear tires of a vehicle traveling in a straight line and deceleration or roadway superelevation are present, the vehicle is almost certain to spin [11-13]. A spin in itself, even if a contact with another vehicle or object is not involved, can be considered a kind of accident.

In [14], an analysis of vehicle loss of control was presented which attempted to correlate the location (front axle vs. rear axle) of worn tires with accident potential. While useful as an initial study, the paper did not address the issue of the running of rear tires in a path or hydrodynamic regime cleared (at least partially) by the front tires, and hence while qualitatively useful, was quantitatively pessimistic in some of its conclusions regarding the effects of worn rear tires on vehicle stability.

In many vehicle handling situations, the rear tires are running in a path at least partially cleared by the front tires. This was examined both theoretically and experimentally in [23]. The experimental program conducted

involved straight running of the test vehicle and no quantitative measurements of wheel spin were taken. Detailed analyses were presented for the cases of hill climbing in a straight line and braking in a straight line.

In the analytical portion of this work, a geometric approach is taken in order to calculate the width of tire contact patch potentially cleared by a leading tire. The approach is valid for cornering maneuvers above and below the vehicle tangent speed, and vehicle geometry, tire characteristics and path are taken into account.

THEORETICAL ANALYSIS

To begin the analysis of hydroplaning during steady-state cornering, some fundamental concepts are needed.

TANGENT SPEED: At very low speeds in a circular cornering maneuver, the rear tires track a smaller radius than the front tires because the vehicle is Ackermann steer, lateral acceleration is zero and no tire slip angles are needed to generate sideforce. Under these conditions, the steering angle required to maintain a desired circular path radius r is purely kinematic, as shown in Figure 1, and is given by:

$$\delta = \tan^{-1}(\ell / r) \cong \frac{\ell}{r} \tag{1}$$

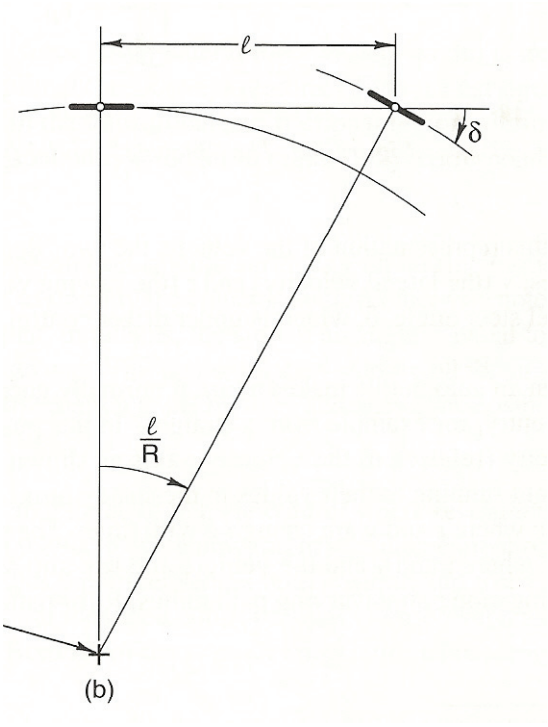

Figure 1: Low-speed Ackermann steer angle

Figure 1 illustrates the so-called bicycle model, and lumps both of the tires on a given axle together, ignoring steer axle Ackermann steering geometry, which can be (a) Ackermann, (b) parallel, or (c) reverse Ackermann, a shown in Figure 2. Passenger cars tend toward parallel or near-parallel geometry, and thus use of the bicycle model is appropriate for the analysis to follow.

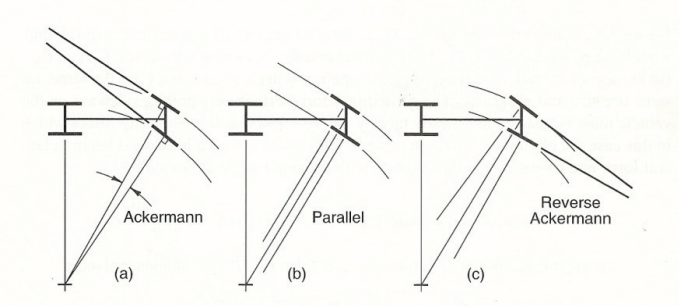

Figure 2: Steered axle geometry

As speed is increased and tire slip angles build to develop the lateral forces needed to resist centrifugal force, body attitude β also increases until, at some speed, the front and rear tires track on circles of the same radius. At this speed, the chassis centerline is tangent to the circular path and the vehicle body attitude angle β, measured at the c.g. of the vehicle, is zero. Above the tangent speed, the rear wheels travel on a larger radius than the front wheels and the vehicle assumes a nose-in attitude. The speed at which β=0 is termed the vehicle tangent speed. Tangent speed is given by [17]:

$$u_t = \sqrt{\frac{-\ell g c C_r}{Wa}} \equiv \sqrt{\frac{-gcC_r}{W_r}} \tag{2}$$

and is independent of turn radius R. Under steady-state Ackermann steer conditions, the radius of the circular arc traveled by the front wheel in Figure 1 is given by:

$$\mathbf{R_f = \frac{\ell}{\sin\left[\tan^{-1}(\ell/R_r)\right]}} \tag{3}$$

For the Ackermann steer angle condition, $\mathbf{R_f > R_r}$. If d is the difference in radii between Rf and Rr:

$$\mathbf{d = \frac{\ell}{\sin\left[\tan^{-1}(\ell/R_r)\right]} - R_r} \tag{4}$$

CALCULATION OF OVERLAP; STRAIGHT RUNNING: We define tire overlap geometrically as shown in the crosshatched area of Figure 3 with dimensions shown in Figure 4:

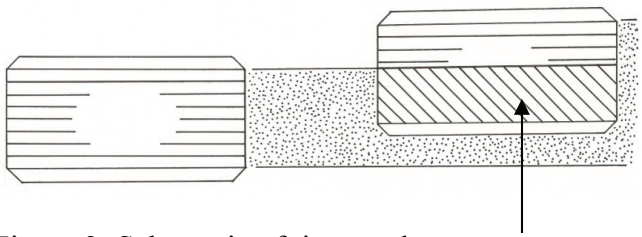

Figure 3: Schematic of tire overlap

The amount of tire overlap will depend on the width of the tire treads and the track width of each axle. For driving in a straight line, $\mathbf{R_f = R_r = \infty}$. The calculation of overlap is straightforward and is given by (see Figure 4; note that TWB > TWA):

$$\mathbf{d_o = \frac{TW_B - TW_A}{2} - (d_1 + d_2)} \tag{5}$$

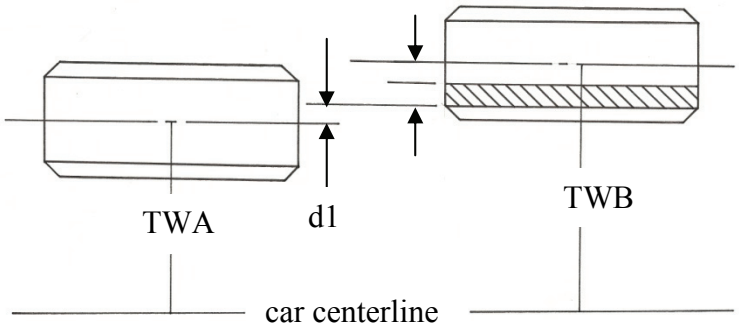

Figure 4: Dimensions used in calculating tire overlap

If do<0, there is no overlap. This could occur if TWB>>TWA and/or different tires are used on each axle.

CALCULATION OF OVERLAP, u ≠ TANGENT SPEED. From the definition of tangent speed, the tires overlap one another and the overlap is 100% if the tires have the same contact patch width and front and rear track widths are equal. If the tire widths and/or track widths are unequal, the calculation of overlap at tangent speed is identical to that for straight running, as given above. If the vehicle is traveling at a speed ≠ its tangent speed, but at a (u,R) pair such that nonzero lateral acceleration exists, the tires must generate sideforces through their slip angles and the sideslip or attitude angle is ≠0 [27]. Figure 5 illustrates the situation for u<ut, when $\beta > 0$; in Figure 6, u>ut and $\beta < 0$ (SAE J670e sign convention).

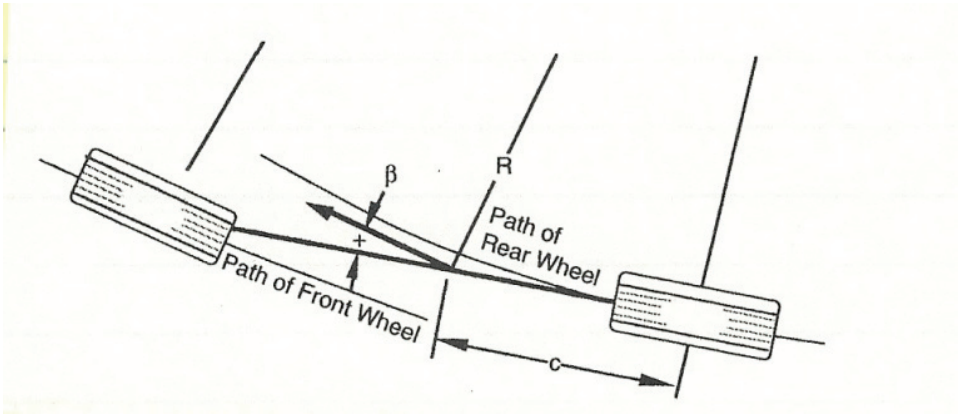

Figure 5: Body attitude angle for u < tangent speed

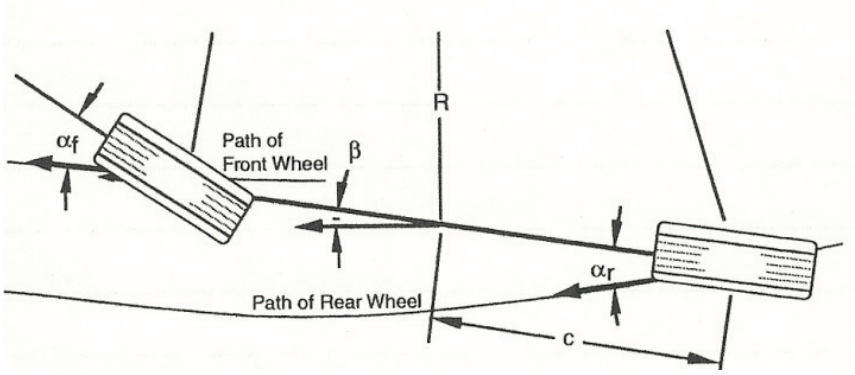

Figure 6: Body attitude angle for u > tangent speed

Body angle is given by:

$$\beta = \frac{57.3c}{R} - \frac{W_f u^2}{C_f R g} \tag{6}$$

Tangent speed does not depend on turn radius, but lateral acceleration and body angle β are f(R,u), as shown in Eq (6). For a given turn radius R and forward velocity u, lateral acceleration is:

$$a_y = \frac{u^2}{R} \tag{7}$$

In order to calculate the amount of overlap, the radii being traversed by the front and rear tire of the bicycle model must be calculated. Rf and Rr can be calculated by using the Law of Cosines:

$$R_r^2 = R^2 + c^2 - 2Rc \times \cos(90 + \beta) \tag{8}$$

$$R_f^2 = R^2 + a^2 - 2Ra \times \cos(90 - \beta) \tag{9}$$

with β in Eqs (8,9) given by Eq (6). For the rear, non-steered tires, the actual radii are easily found by adding and subtracting half the rear track width (TWA or TWB) to Rr. For the front, steered tires, the situation is slightly different, as shown in Figure 7:

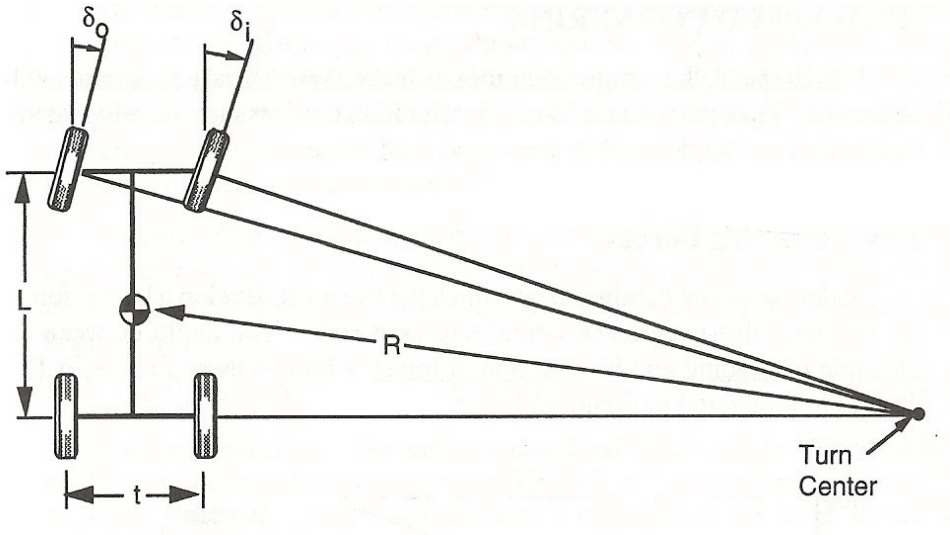

Figure 7: Radii definition for inner and outer steered tires

Figure 7 is drawn assuming that "perfect" Ackermann steer is present, that is, that the inner and outer tire steer angles are such that no scrub is present on either tire; see Figure 2(a) above. This is only possible for a single ℓ,R combination. For all other combinations of ℓ,R one or both tires will exhibit scrub. Much research (e.g., [29]) shows that drivers tend to operate passenger cars in the range $a_y \in [0, \mp 0.4g)$ in normal, non-emergency driving situations of various trip lengths, as shown in Figure 8:

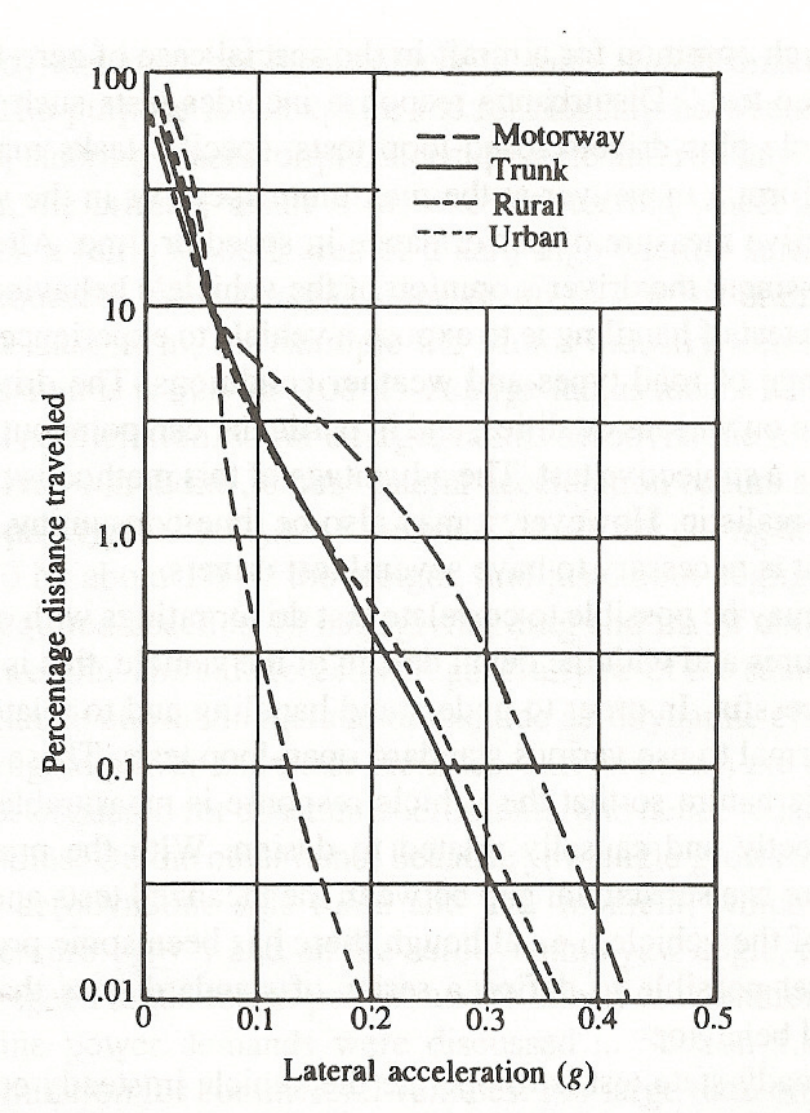

Figure 8: Range of accelerations during normal driving [29]

Within this range, linear tire behavior can safely be assumed, so calculations involving tire characteristics, such as those above performed in Eqs (1-9), can be carried out by modeling tire behavior using only the cornering stiffness coefficient. Most passenger car designs employ near-parallel Ackermann steer (see Figure 2(b) above), and R>>ℓ during all driving maneuvers except for very low speed parking.

Hydroplaning behavior is a phenomenon that is a strong function of vehicle forward velocity u, as shown in Figure 9. Low-speed parking maneuvers are consequently uninteresting in studies of hydroplaning behavior. One approximate expression for determining hydroplaning speed is [15]:

$$u_{hydroplaning}, \text{mph} = 10.35\sqrt{p_o} \tag{10}$$

with inflation pressure po is in units of psi. Numerous other, refined estimates for hydroplaning speed are available, but all show speed dependency.

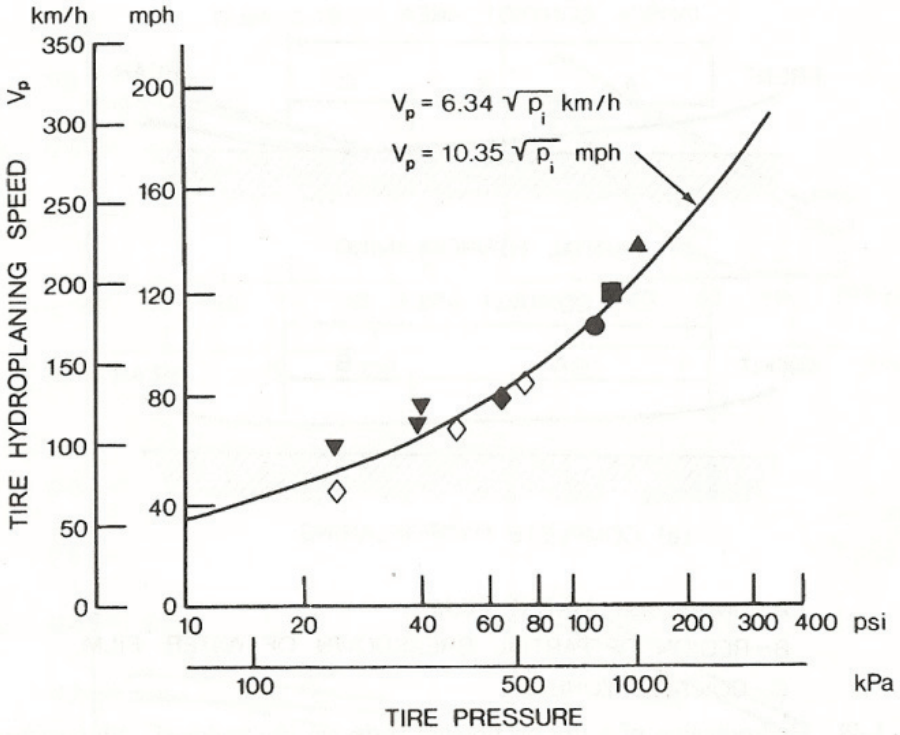

Figure 9: Speed dependency of hydroplaning [31]

With these observations, it is clear that Ackermann steer effects as shown in Figure 2 are negligible, and that calculating overlap for a single tire pair as idealized in the bicycle model is acceptable for the tire pairs on the inside or outside of the curve being traversed. In order to carry out the calculations, vehicle dimensional and inertial data and tire cornering coefficient data are required. All of these can be obtained from [18], as well as from many other sources.

It is straightforward to mechanize the above series of calculations into a spreadsheet; an EXCEL spreadsheet is given at the end of this paper.

SAMPLE CALCULATION: Suppose we consider a 2003-2010 Ford Crown Victoria passenger car. The following data were obtained from [18]:

c=1.73 m ℓ=2.91 m Cf=Cr=789 N/deg

W=17,909 N Wr=7,295 N

TWA=0.80 m TWB=0.83 m

FTW=225 mmRTW=225 mm

Assume a vehicle forward speed of 11.18 m/sec (25 mph) and a turn radius of 60.96 m (200 ft). Then we have the following:

Ackermann steer angle = 2.73 deg.

lateral acceleration = 2.05 m/sec2

front tire slip angle = 2.81 deg

rear tire slip angle = 1.93 deg

tangent speed = 10.24 m/sec

body angle β = -0.31 deg

Under these conditions, the vehicle is operating slightly above its tangent speed (u=109% of ut) and so its body angle $\beta \cong 0$. The rear tire trajectory radius, bicycle model front tire trajectory radius and c.g. radius are essentially identical because the vehicle is traveling so close to its tangent speed. Under this set of conditions, front-rear tire overlap is nearly 100%. Obviously, other combinations of speed, turn radius, vehicle dimensions and tire characteristics produce different overlap conditions.

Repetitive calculations of the type described in the Sample Calculation above show that during typical steady-state cornering undertaken during normal driving maneuvers there is considerable tire overlap. Because of this, situations that involve explanations of cornering performance and vehicle loss of control due to hydroplaning are unrealistic unless they take tire overlap into consideration.

The above calculations do not take into account friction circle budget consumption due to drive effects. For a rear wheel drive vehicle operating on a low-μ surface, the effective traction available at the driven rear wheels is compromised by the need to provide thrust to propel the vehicle. Under these conditions, a vehicle experiment that appears to correlate calculations with a proving ground test may appear to give agreement because of a fortuitous cancellation of effects. This is true to some extent for 4WD vehicles, depending on the front/rear torque split utilized. For front wheel drive vehicles there is no path clearing behavior to account for enhanced tire traction, however.

EXPERIMENTAL PROGRAM

An experimental program was conducted to examine the qualitative effects of front wheel path clearing. A 2005 Ford Crown Victoria (VIN 2FAFP71W45X150970) police interceptor vehicle and a 2007 Chevrolet Suburban SUV (VIN 1GNFK16398J240768) were instrumented with a VBox © model VBoxIISX data acquisition system (20 Hz sample rate), allowing measurement of vehicle position, velocity & acceleration. Relative (unscaled) wheelspeed data were also captured by the VBox from the vehicle CAN bus and ABS wheel sensors for the Ford Crown Victoria test vehcle.

Straight line maximum-intensity braking maneuvers were chosen for the experimental program because the path clearing effect described above can most easily be experimentally evaluated during straight-line behavior. During a straight line braking test, the front and rear tracks on both sides of the test vehicles are constantly superimposed one over the other, as shown in Figure 3. Tire relative alignment for the test maneuvers thus remained constant and repeatable from test to test. Driver workload and control capability and requirements are also minimized during straight line testing.

For example, for the Ford Crown Victoria police interceptor test vehicle, the front and rear track widths are 62.8" and 65.6" respectively. This means that there is an uncleared strip on the outside edge of each rear tire of:

$$\frac{65.6-62.8}{2} = 1.2'' \qquad (11)$$

The loaded width of the tire contact patch was measured as 8.9". Thus 87% of the contact patch width of the rear tires is running in the path taken by the front tires when the vehicle is traveling in a straight line:

$$\frac{8.9-1.2}{8.9} \times 100 = 87\% \tag{12}$$

Tests were conducted on smooth, level asphalt (dry sliding μ-value ~ 0.84) under both wet and dry conditions. Differences in front/rear wheel rpm, and thus local hydroplaning of each individual wheel, were reflected in the amount of ABS cycling that occurred during the braking maneuvers, as measured by CAN bus wheelspeed data. High speed videography was also utilized to examine wheel rpm behavior.

Water depth could not be accurately controlled during the wet braking experiments. To ensure hydroplaning potential, the test surface was flooded immediately prior to each wet test using a fire truck with a large-capacity rear gate. The delay between surface wetting and the conducting of the actual test was kept to less than one minute. Estimates of water depth d during testing are in the range of $d \in [0.1, 0.2"]$, a significant, deep depth unlikely to be reached on a public roadway without a downpour occurrence and/or heavily rutted pavement, together with light traffic. The tires used for all tests were essentially new but were lightly scrubbed prior to testing in order to remove mold flash. During all tests, the driver was instructed to use fixed steering control. The test drivers were all highly experienced Wisconsin State Patrol accident reconstructionists. Tests were conducted with normal tire pressures at all four wheels (32 psi), and also with reduced tire pressure (15 psi) on all four wheels of the test vehicles. A total of seven dry tests and 15 wet tests were successfully conducted, though there were many other tests for which some of the data were not captured for various reasons. The test drivers had extensive experience in the use of ABS braking systems, and were able to successfully activate the ABS systems during both wet and dry testing.

Figure 10 shows a pre-test flooding operation in progress.

Figure 10: Test surface flooding operation

Figures 11 and 12 display the two test vehicles during wet test operation

Figure 11: Chevrolet Suburban wet braking test. Note visible vehicle tracks.

Figure 12: Ford Crown Victoria wet braking test. Note visible vehicle tracks.

Because of rear-to-front weight transfer during deceleration and path clearing, each axle of the vehicle experiences two competing tractive effects during braking maneuvers. The effects tend to offset one another.

The front wheels of the vehicle have their dynamic vertical loading Fz increased due to rear-to-front weight transfer, but they are operating in deeper, undisturbed water and thus more likely to experience hydroplaning. Conversely, the rear wheel vertical loads are reduced through rear-to-front weight transfer, but they are running in paths mostly cleared by the front wheels, and thus their propensity to hydroplane is reduced.

Under dry braking conditions (when the tire/road μ-values would be nearly the same for all four wheels), rear-to-front weight transfer would lead to increased rear axle ABS cycling as deceleration rates and rear-to-front weight transfer increased. The issue during the test sequence was to determine if this would be the case under wet/hydroplaning situations with path clearing. If path clearing is able to increase the rear axle tire/road μ-value when compared to that of the front axle, then rear axle ABS cycling will be reduced. Under these circumstances, the rear tire friction circle (radius = μFz) will increase.

During a typical test, following a wide open throttle acceleration, braking initiation occurred at speeds in the range of $u \in [50, 60\ \text{mph}]$ at ~ 400 ft. from the starting point, as shown in Figure 13.

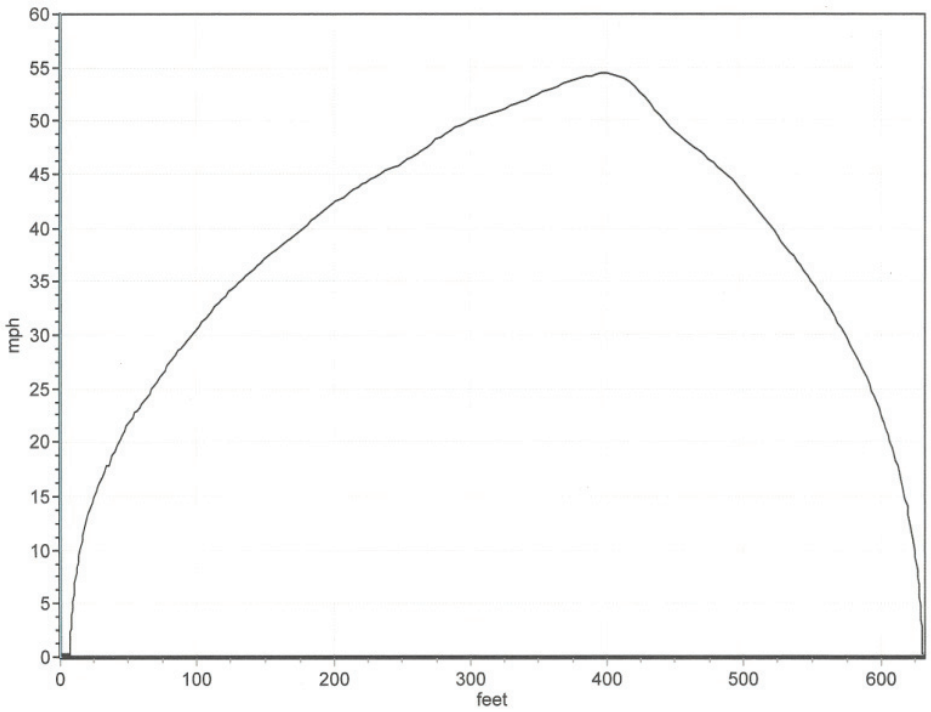

Figure 13: Typical velocity vs. distance VBoxIISX trace

Wet pavement deceleration rates averaged ~ 0.4g while dry pavement deceleration rates were ~ 0.85g. For example, with the Ford Crown Victoria dimensions given in the Appendix, a wet deceleration of 0.4g produces a fractional load transfer (FLT) of:

$$FLT = \frac{2 \times 0.4 \times 25}{114.6} = 0.175 \tag{13}$$

This amount of FLT produces a total rear-to-front weight shift of:

$$\Delta W = 0.175 \times 4{,}200 = 735 \text{ lbf} \quad (14)$$

Thus, the static axle loads of 2,489/1711 become dynamic axle loads of 2,489+735=3,224 lbf front and 1711-735=976 rear during the wet braking experiments. With these axle loads, ABS actuation at the rear wheels would be expected to be relatively easy to achieve unless the wheels are running on a surface with larger tire/road μ-values that the front wheels due to path clearing.

TEST RESULTS

DRY TESTING RESULTS: Figure 14 shows the results of one of the tests performed on dry pavement. In this test, all four tire pressures on the Ford Crown Victoria police interceptor test vehicle were at their nominal value (32 psi). Wheel rpm for both right side wheels smoothly increases in tandem during the acceleration portion of the test, but differs during the deceleration phase due to ABS cycling.

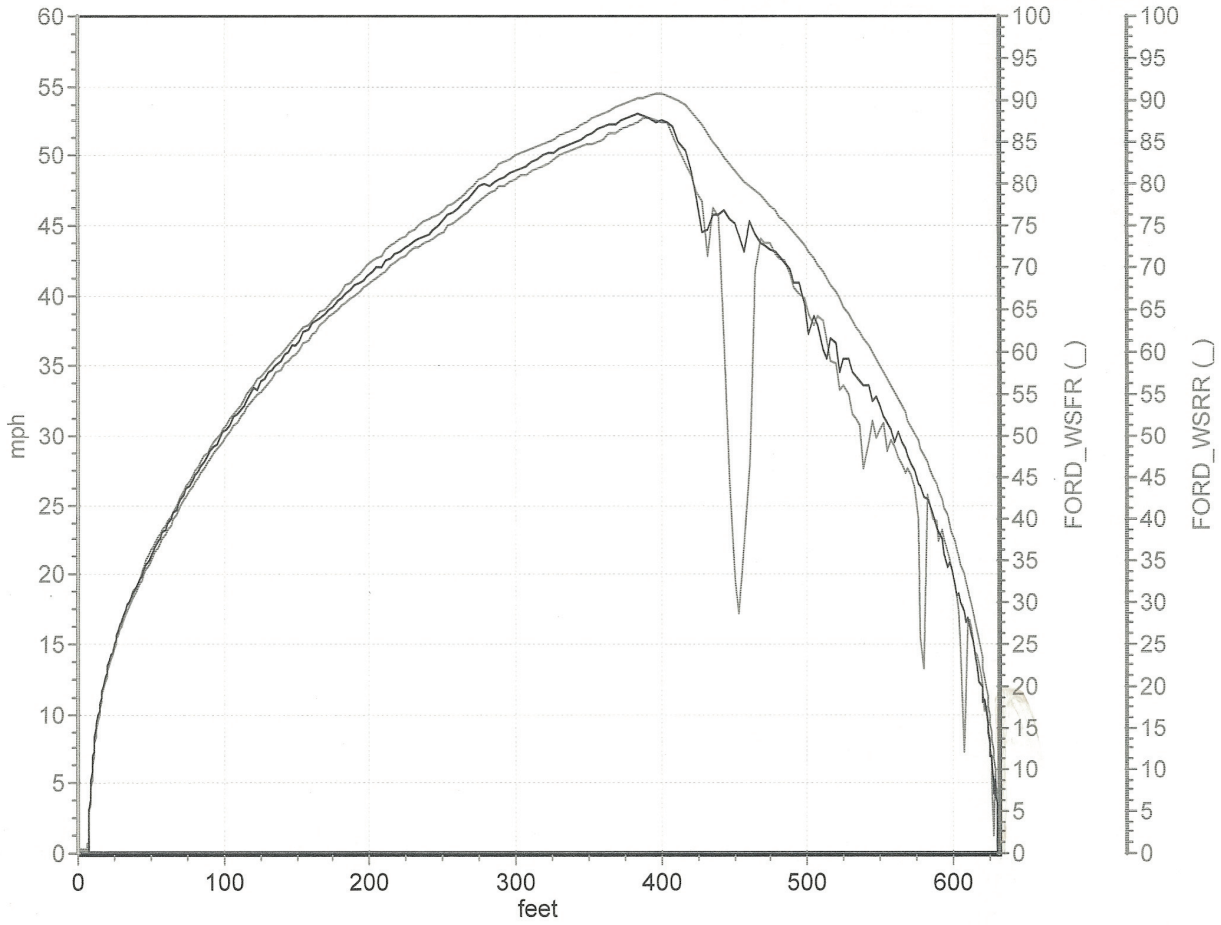

Figure 14: Dry pavement test No. 2, all tires at 32 psi

Figure 14 shows right side wheel rpm unscaled values as functions of distance for the Ford Crown Victoria police interceptor test vehicle. Some ABS cycling of both the right front (WSFR) and right rear (WSRR) wheels was noted during the test on this high-μ dry surface, though the right rear ABS cycling was considerably less than that experienced at the right front wheel.

WET TEST RESULTS WITH NORMAL TIRE PRESSURES: Figure 15 presents results very similar to those shown in Figure Seven except that the pavement was wet. The test vehicle was the same Ford Crown Victoria police interceptor and all tires were at 32 psi.

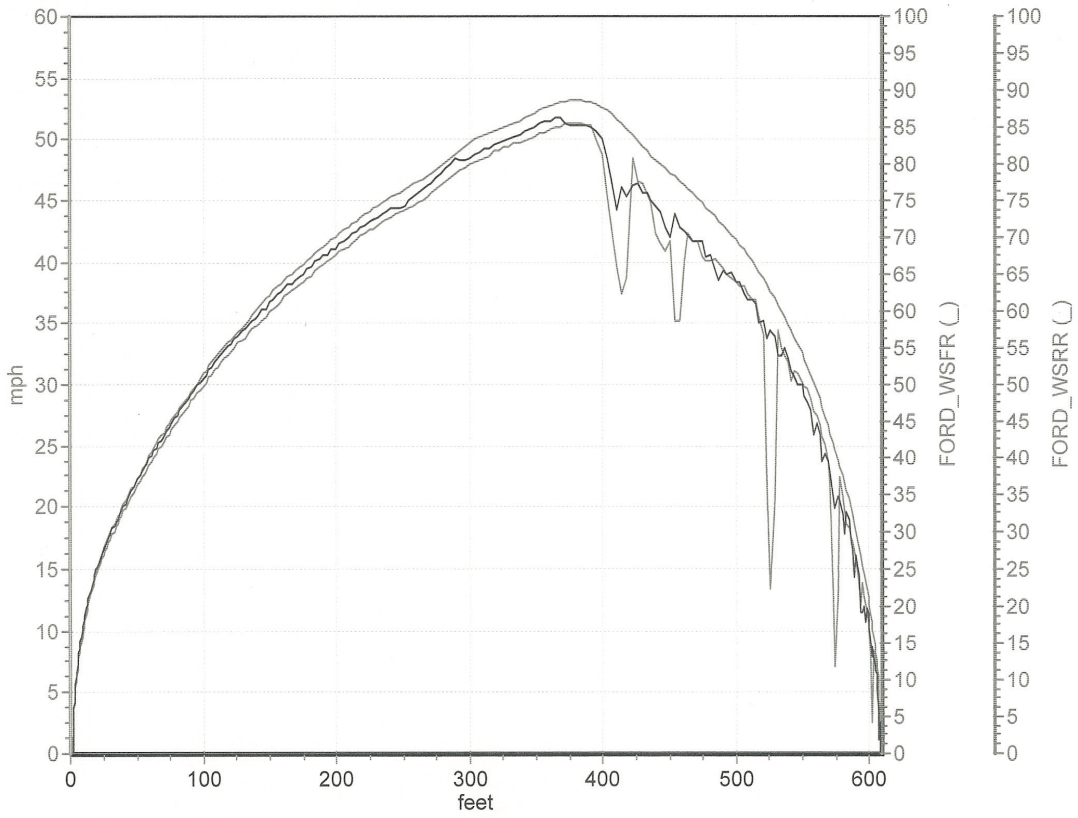

Figure 15: Wet pavement test No. 38, all tires at 32 psi

Figure 15 shows significant ABS activity at the right front wheel and essentially no ABS cycling at the right rear wheel, and demonstrates that the right front wheel cleared a path for the right rear wheel that produced a much higher tire/road μ-value for that rear tire. Stopping distances in Figures 14 & 15 are quite close, indicating that, as expected, most braking takes place at the front wheels. All other tests showed similar results. Numerical integration (simple Euler integration used) of the difference between vehicle speed and wheel speed signals gave the following results:

Figure 14, Test 2: rear wheel integral=48.9 units

Figure 15, Test 38: rear wheel integral=36.7 units or 24.9% less

These results indicate that the clearing hypothesis is qualitatively valid when tire pressures are at their recommended values.

WET TEST RESULTS WITH REDUCED TIRE PRESSURES: Figures 16 shows right side wheel rpm test results for wet pavement with reduced tire pressure of 15 psi at all four wheels.

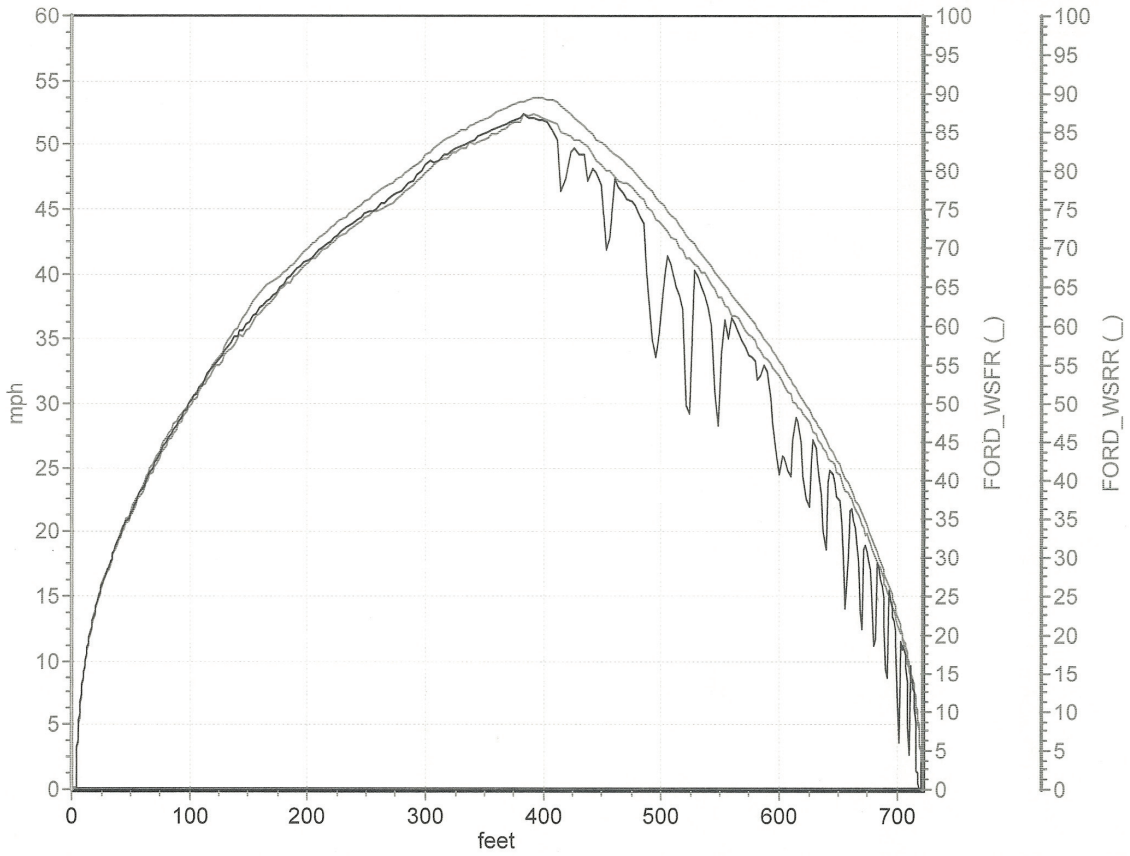

Figure 16: Wet pavement test No. 33, all tires at 15 psi

Figure 16 shows different characteristics for wheel rpm values than those obtained in Figures 14 and 15 for normal inflation pressures. Instead of ABS cycling at the front wheel and little at the rear wheel, the pattern of tire behavior is completely reversed.

It is well-known that the shape and size of the tire contact patch and the normal pressure distribution it experiences are strong functions of inflation pressure [25,26,27]. It is intuitive that greater inflation pressures will reduce the contact patch area, thus requiring higher local pressures to support a given vertical load. This relationship was originally approximately expressed in [28] as:

$$u_{hydroplaning} = 10.35\sqrt{p} \tag{15}$$

In Eq (15), u = minimum speed for hydroplaning in mph and p = inflation pressure in mph. Many more sophisticated relationships have been developed since the publication of [28], but all show essentially the same trend: hydroplaning speed decreases with decreasing tire pressure. With reduced tire pressures, test results indicate that the rear wheels of the vehicle do not generate sufficient local pressure underneath the tire to eject water, even when they are running in a path cleared by the front tire. Because of this, the rear tire ABS behavior shows nearly continuous cycling during the braking maneuver depicted in Figure 16.

As mentioned above, a Chevrolet Suburban was also used as a test vehicle. Results from that vehicle were essentially identical to those obtained during testing of the Ford Crown Victoria test vehicle.

CONCLUSIONS AND DISCUSSION

CONCLUSIONS: The theoretical calculations and test program results indicate that:

1. When tires are normally inflated, the front tires clear a path for the rear tires and significantly reduce the tendency for the wheels running in the cleared path to hydroplane. The results shown in [14] for the vehicle handling effects of rear wheel hydroplaning are therefore overly pessimistic for many situations, especially those that involve either straight line braking and/or acceleration, or steady-state cornering at or near the vehicle tangent speed.

2. When the tires running in a cleared path are at reduced inflation pressure, the clearing effect of the front tires is attenuated.

3. Path clearing for tires with cross-sectional profiles different than those used on automobiles and over-the-road trucks may not behave in a manner similar to the behavior reported here. For example, motorcycle tires have a semicircular cross section and exhibit elliptical contact area as shown in Figures 17 and 18:

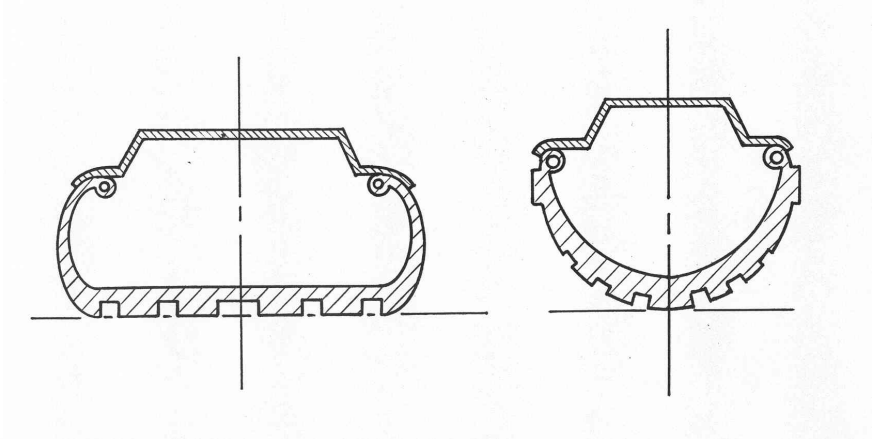

Figure 17: Cross-section of car/truck tire vs. motorcycle tire

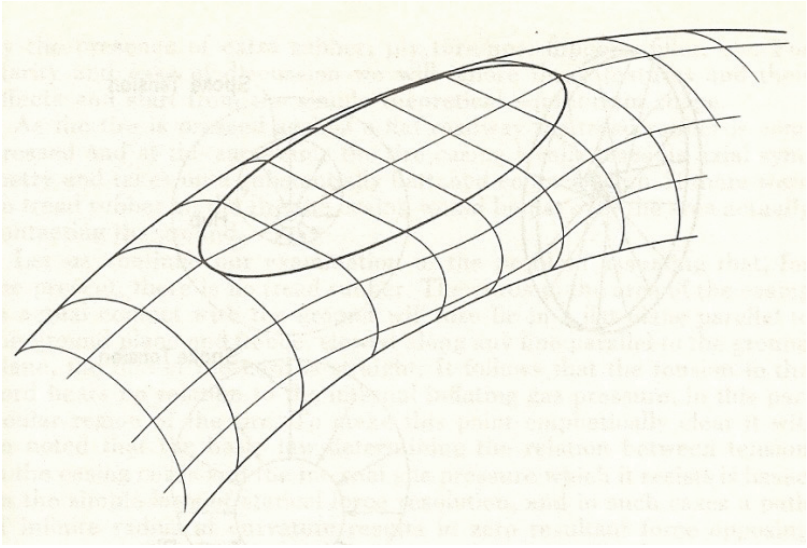

Figure 18: Elliptical contact patch of motorcycle tire

DISCUSSION: The path clearing effect described above was successfully demonstrated in the ABS activity of the wheels and in videotapes of the experimental maneuvers. Future research in this area has to be concentrated on the following areas:

1. Examination of the sensitivity of path clearing as a function of tire inflation pressure and tread depth [24].

2. Examination of the sensitivity of path clearing to pavement macrotexture density [8,9,20,21].

3. Behavior of tires with different cross-sectional properties, as described in Figures 10 and 11.

4. Experiments conducted at lower and higher initial speeds.

While the focus of the experiments and theoretical calculations made was on hydroplaning situations, it is possible that path disturbance (as opposed to path "clearing") may occur during terramechanics involved with off-road excursions. No investigations have been conducted along these lines.

REFERENCES

1. Browne, A.L., “Mathematical Analysis for Pneumatic Tire Hydroplaning,” in Surface Texture v. Skidding: Measurements, Frictional Aspects and Safety Features of Tire-Pavement Interactions, ASTM STP 583, American Society for Testing and Materials, pp. 75-94 (1975).

2. Veith, A.G. and Pottinger, M.G., “Tire Wet Traction: Operational Severity and its Influence on Performance,” The Physics of Tire Traction, (D.F. Hays & A.L. Browne, Ed.), Plenum Press, New York, NY, pp. 5-20 (1974).

3. Kelley, J.D., Jr., “Factors Affecting Passenger Tire Traction on the Wet Road,” SAE Paper No. 680138 (1968).

4. Staughton, G.C., “The Effect of Tread Pattern Depth on Skidding Resistance,” Road Research Laboratory Report LR323, Ministry of Transport, Great Britian (1970).

5. Sabey, B.E., Williams, T. & Lupton, G.N., “Factors Affecting the Friction of Tires on Wet Roads,” SAE paper No. 700376 (1970).

6. Bergman, W., Clemett, H.R. & Sheth, N.J., “Tire Traction Measurements on the Road and in the Laboratory,” SAE Paper No. 710630 (1970).

7. Lippman, S.A. & Oblizajek, K.L., “The Influence of Tire Wear on Steering Properties and the Corresponding Stresses at the Tread-Road Interface,” SAE Paper No. 741102 (1970).

8. Agrawal, S.K. & Henry, J.J., “A Technique for Evaluating the Hydroplaning Potential of Pavements,” Transportation Research Board, 56th Annual Meeting, Washington, D.C. (1977).

9. Gallaway, B.M., et al., “Pavement and Geometric Design Criteria for Minimizing Hydroplaning,” Final Report Contract No. DOT-FH-11-8269, Report No. FHWA-RD-79-31, Federal Highway Administration, Washington, D.C. (1979).

10. Wohanka, U. & Essers, U., “Influence of Waterfilm Thickness on Tyre Force and Moment Characteristics Measured on Public Roads,” European Automobile Engineers Cooperation, 5th International Congress, Strasbourg, France (1995).

11. Sakai, H., Kanaya, O. & Ikayama, T., “The Effect of Hydroplaning on the Dynamic Characteristics of Car, Truck and Bus Tires,” SAE paper No. 780195 (1978).

12. Hayes, G.G., Ivey, D.L. & Gallaway, B.M., “Hydroplaning, Hydrodynamic Drag and Vehicle Stability,” in Frictional Interaction of Tire and Pavement, ASTM STP 793 (W.E. Meyer & J.D. Walter, Eds.), American Society for Testing and Materials, pp. 151-166 (1983).

13. Allen, R.W., et al., “Characteristics Influencing Ground Vehicle Lateral/Directional Dynamic Stability,” SAE Paper No. 910234 (1991).

14. Blythe, W. & Day, T.D., “Single Vehicle Wet Road Loss of Control; Effects of Tire Tread Depth and Placement,” SAE Paper No. 2002-01-0553 (2002).

15. Clark, S.K. (Ed.), Mechanics of Pneumatic Tires, National Bureau of Standards Monograph No. 122, p. 469 (1971).

16. Horne, W.B. et al., “Recent Research on Ways to improve Tire Traction on Water, Slush or Ice,” AIAA Aircraft Design & Technology Meeting, Los Angeles, CA (1965).

17. Milliken, W.F., Jr. & Milliken, D.L., Race Car Vehicle Dynamics, Society of Automotive Engineers, 400 Commonwealth Drive, Warrendale, PA 15096.0001, ISBN 1-56091-526-9, pp. 174-175 (1995).

18. _____ HVE (Human-Vehicle-Environment) Simulation Software, Engineering Dynamics Corp., 8625 S.W. Cascade Boulevard, Suite 200, Beaverton, OR 97008.7100, http://www.edccorp.com (various dates)

19. Day, T.D., “Validation of the EDVSM 3-dimensional Vehicle Simulator,” SAE Paper No. 970958 (1997).

20. _____, SAE J266, Passenger Car and Light Truck Direction Control Response Test Procedures, Society of Automotive Engineers, 400 Commonwealth Drive, Warrendale, PA 15096.0001, http://www.sae.org (various dates).

21. Baker, J.S., Traffic Accident Investigation Manual, The Traffic Institute, Northwestern University, Evanston, IL, ISBN 0-912642-01-7, p. 210, Exhibit 9-5 (1975).

22. _____ASTM E 965-96, Standard Test Method for Measuring Pavement Macrotexture Depth Using a Volumetric Technique (latest version).

23. Metz, L. D., “Realistic Rear Axle Hydroplaning during Forward Motion,” SAE Paper No. 2006-01-1560 (2006).

24. _____, SAE J670e, Vehicle Dynamics Terminology, Definition §7.5.1. (latest version).

25. Williams, A. R. & Evans, M. S., “Influence of Tread Wear Irregularity on Wet Friction Performance of Tires,” Frictional Interaction of Tire and Pavement, ASTM STP 793, pp. 41-64 (1983).

26. Milliken, W.F., Jr. & Milliken, D.L., Op. cit., p. 76, Figure 2.42.

27. _____, SAE J670e, Vehicle Dynamics Terminology, Definition §8.4.4. (latest version).

28. Milliken, W.F., Jr. & Milliken, D.L., Op. cit., p. 150.

29. Dixon, J. C., Tires, Suspension and Handling (2nd Ed.), Society of Automotive Engineers, 400 Commonwealth Drive, Warrendale, PA 15096.0001, ISBN 1-56091-831-4, P. 55, Fig. 1.12.1 (1996).

30. Smith, J. G. & Smith, J. E., Lateral Forces on Vehicles during Driving, Automobile Engineer (1967).

31. Wong, J. Y. Theory of Ground Vehicles (3rd Ed.), John Wiley & Sons, Inc., New York, NY, ISBN 0-471-35461-9, P. 70, Figure 1.50 (2001).

CONTACT INFORMATION

The Author can be contacted at Metz Engineering and Racing, LLC, 1108 W. William Street, Champaign, IL 61821.4507, (01)217.351.6070 (voice+fax), (01)217.419.1611 (mobile), indydoc@uiuc.edu.

DEFINITIONS/ABBREVIATIONS

Symbol	Definition (units)
c	distance from c.g. to rear axle (L)
ℓ	wheelbase=a+b (L)
W	vehicle curb weight (F)
Wf	weight on front axle (F)
Wr	weight on rear axle (F)
R	turn radius at c.g. of vehicle (L)
Rf	turn radius at front axle (L)
Rr	turn radius at rear axle (L)
ut	tangent speed (L/T)
u	forward velocity (L/T)
v	lateral velocity (L/T)
Cf	front tire cornering stiffness (F/deg.)
Cr	rear tire cornering stiffness (F/deg.)
TWA	smaller axle track width (L)
TWB	larger axle track width (L)

FTW	front tire contact patch width (l)
RTW	rear tire contact patch width (L)
g	acceleration of gravity (L/T2)
ay	lateral acceleration (L/T2)

Metz Engineering and Racing
L. Daniel Metz, Ph.D., P.E.
1108 West William St., Champaign, IL 61821.4507
phone/fax 217.351.6070 INDYDOC@UIUC.EDU
www.metzengandracing.com

STEADY-STATE HANDLING CALCULATIONS
2-degree-of-freedom bicycle model

Car= 2003-2010 Ford Crown Victoria

	U.S. 1		U.S. 2		S.I.	
a=	46.68	in	3.89	ft	1.19	meters
c=	67.92	in	5.66	ft	1.73	meters
L=	114.60	in	9.55	ft	2.91	meters
Cf=	177.40	lbf/deg			789.08	N/deg
Cr=	177.40	lbf/deg			789.08	N/deg
W=	4026.29	lbf			17908.94	N
Wf=	2386.26	lbf			10614.09	N
Wr=	1640.03	lbf			7294.84	N
front track=	31.40	in	2.62	ft	0.80	meters
rear track=	32.80	in	2.73	ft	0.83	meters
front tire width=	225.00	mm	0.74	ft	0.23	meters
reasr tire width=	225.00	mm	0.74	ft	0.23	meters
u=	25.00	mph	36.67	ft/sec	11.18	m/sec
R=	200.00	ft			60.96	m

		U.S. 1		U.S. 2		S.I.	
ok	Ackermann steer angle=	2.73	deg				
ok	lateral acceleration=	6.72	ft/sec^2	0.21	g	2.05	m/sec^2
ok sign	front tire slip angle=	2.81	deg				
ok sign	rear tire slip angle=	1.93	deg				
ok sign	steer angle=	3.62	deg				
ok sign	body angle beta=	-0.31	deg				
ok sign	tangent speed=	33.59	ft/sec	22.91	mph	10.24	m/sec
	critical speed=	#NUM!	ft/sec	#NUM!	mph	#NUM!	m/sec
	characteristic speed=	64.69	ft/sec	44.1075	mph	19.72	m/sec
	static margin=	0.09	ft			0.03	m
	neutral steer point=	0.50	ft			0.15	m
	understeer gradient=	4.21	deg/g			1.28	m

** exists only for OS car

STABILITY DERIVATIVES

	Y sub-beta =	-354.80
	Y sub-r =	8.56
ok	Y sub-delta =	177.40
	N sub-beta =	314.00
	N sub-r =	228.21
	N sub-delta =	-690.09

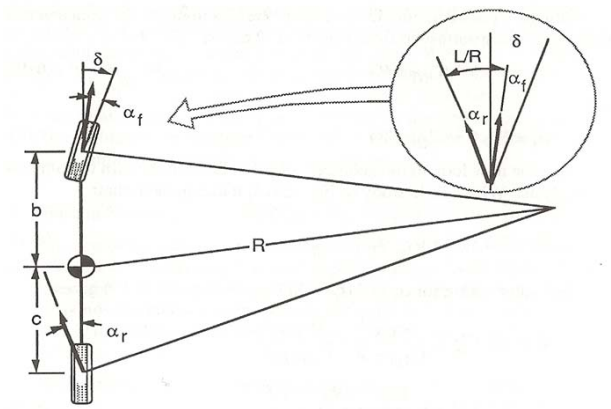

	U.S.1		U.S. 2		S.I.	
bicycle rear tire radius=	200.0494	ft			60.9751	
bicycle front tire radius=	200.0589	ft			60.9779	
outside rear tire radius=	202.7828	ft			61.8082	
inside rear tire radius=	197.3161	ft			60.1419	
outside front tire radius=	202.6755	ft			61.7755	
inside front tire radius=	197.4422	ft			60.1804	
overlap=	0.6310	ft	7.5716	inches	19.2319	cm
% overlap=	85.4749	percent				